Introduction

Oil and gas exploration requires the establishment of accurate seismic wave velocity model so as to achieve accurate imaging and time-depth conversion. In order to analyze seismic wave type, seismic wave field characteristics and understand complex near surface impact on exploration targets, the free-surface boundary condition must be satisfied at the top boundary of the model.

In the last decades, various approaches have been proposed for simulating the propagation of elastic waves with free boundaries. These includes finite element method, spectral element method, pseudo spectral method, boundary element method and finite difference method, each of them have different adaptability and advantages. Coarse grid method like high-order finite difference method is ideally suited for implementing fast, memory efficient and paralleled 2-D and 3-D elastic modeling schemes. Topography poses a problem for finite difference method. For the free surface boundary condition, a variety of methods of free surface boundary condition approximate schemes (Levander, 1988; Jih et al., 1988; Hestholm et al., 1994; Robertsson, 1996; Ohminato et al., 1997; Mittet, 2002; Wang et al., 2004) have been developed in finite difference forward simulation.

The present studies of the free-surface condition are concerned with the more general isotropic cases. This paper extends the image method from the existing elastic/viscoelastic isotropic media model to anisotropic media model. This new method is simple to implement in conventional staggered finite difference schemes, is computationally efficient and enables modeling of highly irregular topography.

Formulation of Anisotropic Wave Modeling

In the 2D3C anisotropic case, elastic wave propagation is described by a set of coupled partial differential equations for stress and velocity:

$$\begin{cases} \dfrac{\partial \upsilon_x}{\partial t} = \dfrac{1}{\rho}\left(\dfrac{\partial \sigma_{xx}}{\partial x} + \dfrac{\partial \sigma_{xz}}{\partial z}\right) \\ \dfrac{\partial \upsilon_y}{\partial t} = \dfrac{1}{\rho}\left(\dfrac{\partial \sigma_{xy}}{\partial x} + \dfrac{\partial \sigma_{yz}}{\partial z}\right) \\ \dfrac{\partial \upsilon_z}{\partial t} = \dfrac{1}{\rho}\left(\dfrac{\partial \sigma_{zx}}{\partial x} + \dfrac{\partial \sigma_{zz}}{\partial z}\right) \end{cases} \tag{1}$$

$$\begin{cases} \dfrac{\partial \sigma_{xx}}{\partial t} = C'_{11}\dfrac{\partial \upsilon_x}{\partial x} + C'_{13}\dfrac{\partial \upsilon_z}{\partial z} + C'_{14}\dfrac{\partial \upsilon_y}{\partial z} + C'_{15}\left(\dfrac{\partial \upsilon_x}{\partial z} + \dfrac{\partial \upsilon_z}{\partial x}\right) + C'_{16}\dfrac{\partial \upsilon_y}{\partial x} \\ \dfrac{\partial \sigma_{zz}}{\partial t} = C'_{13}\dfrac{\partial \upsilon_x}{\partial x} + C'_{33}\dfrac{\partial \upsilon_z}{\partial z} + C'_{34}\dfrac{\partial \upsilon_y}{\partial z} + C'_{35}\left(\dfrac{\partial \upsilon_x}{\partial z} + \dfrac{\partial \upsilon_z}{\partial x}\right) + C'_{36}\dfrac{\partial \upsilon_y}{\partial x} \\ \dfrac{\partial \sigma_{yz}}{\partial t} = C'_{14}\dfrac{\partial \upsilon_x}{\partial x} + C'_{34}\dfrac{\partial \upsilon_z}{\partial z} + C'_{44}\dfrac{\partial \upsilon_y}{\partial z} + C'_{45}\left(\dfrac{\partial \upsilon_x}{\partial z} + \dfrac{\partial \upsilon_z}{\partial x}\right) + C'_{46}\dfrac{\partial \upsilon_y}{\partial x} \\ \dfrac{\partial \sigma_{xz}}{\partial t} = C'_{15}\dfrac{\partial \upsilon_x}{\partial x} + C'_{35}\dfrac{\partial \upsilon_z}{\partial z} + C'_{45}\dfrac{\partial \upsilon_y}{\partial z} + C'_{55}\left(\dfrac{\partial \upsilon_x}{\partial z} + \dfrac{\partial \upsilon_z}{\partial x}\right) + C'_{56}\dfrac{\partial \upsilon_y}{\partial x} \\ \dfrac{\partial \sigma_{xy}}{\partial t} = C'_{16}\dfrac{\partial \upsilon_x}{\partial x} + C'_{36}\dfrac{\partial \upsilon_z}{\partial z} + C'_{46}\dfrac{\partial \upsilon_y}{\partial z} + C'_{56}\left(\dfrac{\partial \upsilon_x}{\partial z} + \dfrac{\partial \upsilon_z}{\partial x}\right) + C'_{66}\dfrac{\partial \upsilon_y}{\partial x} \end{cases} \tag{2}$$

where C' is the rotation matrix, ρ is the density, σ_{ij} are the stress; υ_x, υ_y and υ_z are the velocity components.

Implementation of Free Surface Condition with Surface Topography

The system of equation (1) and (2) is easily solved using a staggered grid finite difference technique. Figure 1 illustrates the layout of the wave field variables and media parameters on the staggered grid mesh.

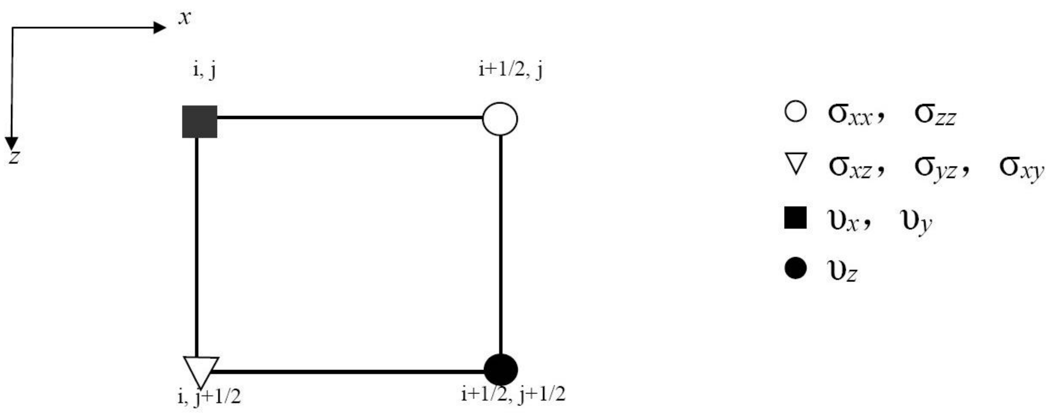

***Figure 1** Grid layout for staggered grid formulation. The indices (i,j) represent values of the spatial coordinates (x,z), respectively.*

The implementation in equation (1) and (2) works fine for the internal part of the model, including water and solid interfaces. However, the free surface need special considerations. In nature, the stress components σ_{zz} , σ_{yz} and σ_{xz} on the earth's surface are actually close to zero, we need to modify the staggered grid scheme for the free surface in order to have a proper behavior of the elastic field. All field components and media parameters are assumed to be zero above the free surface. The trivial boundary condition is that the normal stress component is zero on the free surface and shear stress component is also zero on the free surface. However, it is impossible to implement the stress components satisfy the discussed boundary conditions at one level in staggered grids since the normal and shear stresses are not defined at the same level.

The boundary treatment described in this section is based on the idea developed by (Robertsson et al, 1996 and Wang et al, 2004) for the isotropic elastic wave modeling. For the imaging method, both normal and shear stress components at a free surface are odd functions and this allows them to be zero at the free surface. We set the free surface passes through the grid points at the location of shear stress components. For the flat free surface case, the improved method implemented in the 4th-order staggered grid formulation can be written as follows:

$$\begin{cases} \sigma_{xy}(i,j)=0 \\ \sigma_{yz}(i,j)=0 \\ \sigma_{xz}(i,j)=0 \\ \sigma_{xz}(i,j-1)=-\sigma_{xz}(i,j+1) \\ \sigma_{xz}(i,j-2)=-\sigma_{xz}(i,j+2) \\ \sigma_{zz}(i,j)=-\sigma_{zz}(i,j+1) \\ \sigma_{zz}(i,j-1)=-\sigma_{zz}(i,j+2) \end{cases} \tag{3}$$

If the free surface is located through the υ_z, σ_{xz}, σ_{xy} and σ_{yz} components, while the normal stresses and the corresponding memory variables are located in the air above the free surface. The formulation can be written as follows:

$$\begin{cases} \sigma_{xy}(i,j)=0 \\ \sigma_{yz}(i,j)=0 \\ \sigma_{xz}(i,j)=0 \\ \sigma_{xz}(i+1,j)=-\sigma_{xz}(i-1,j) \\ \sigma_{xz}(i+2,j)=-\sigma_{xz}(i-2,j) \end{cases} \tag{4}$$

Numerical Example

Two simulations were performed using the model described in Figure 2. The model is 6000*m* width by 3000*m* depth. A Gauss wavelet with a center frequency of 30Hz was used as a pure *P*-wave source. The source is buried at (3000*m*, 40*m*). The step lengths are Δx=10*m* and Δz=5*m*, respectively. The sampling interval is 2*ms*. The record length is 5000*ms*.

In the first simulation, the first interface in the model was ignored, so that the entire model upon the varying topography is same with the material properties of the first layer. For the second simulation, the model as described by Figure 2 was used. Comparisons of the snapshots of the particle velocity from two simulations at the instant 140*ms* are shown in Figure 3a and Figure 3b. Irregular free surface makes the wave field complicated including scattering and multiple reflections. The anisotropic nature of the wave field is evident, the S_υ conversion, triplicating direct S_υ wave and Rayleigh wave at the free surface. Anisotropic properties of the media makes the wave field more complicated. Figure 4 shows the *x* component of the surface seismogram recorded for the two simulations. The various converted reflections, diffractions, and direct waves including the Rayleigh wave are present.

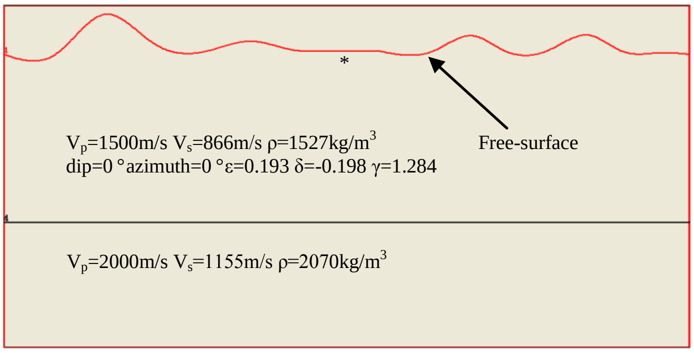

***Figure 2** The irregular free surface model. The star denotes the location of the 30Hz Gauss wavelet source.*

a)

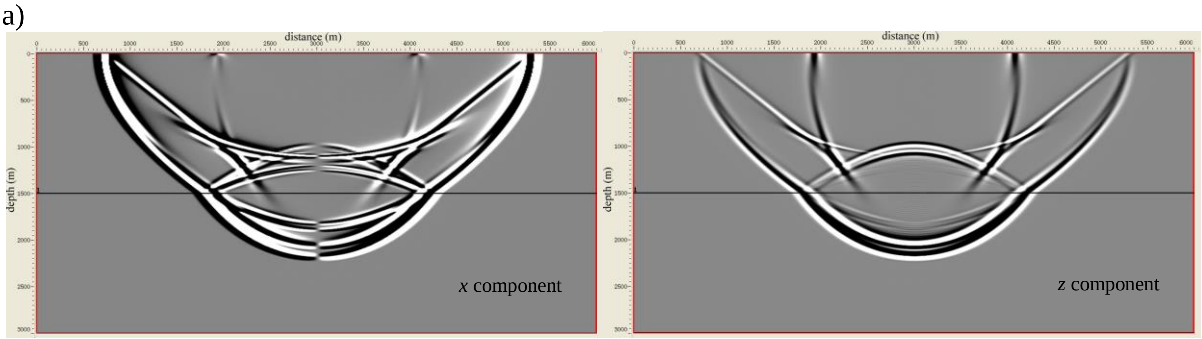

b)

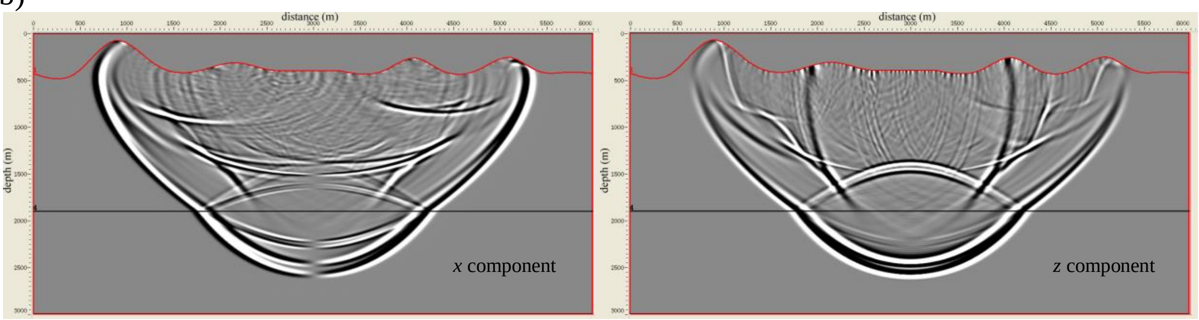

***Figure 3** Snapshots of x and z components of particle velocity for elastic anisotropic wave propagation in a complex model. (a) the first simulation. (b) the second simulation.*

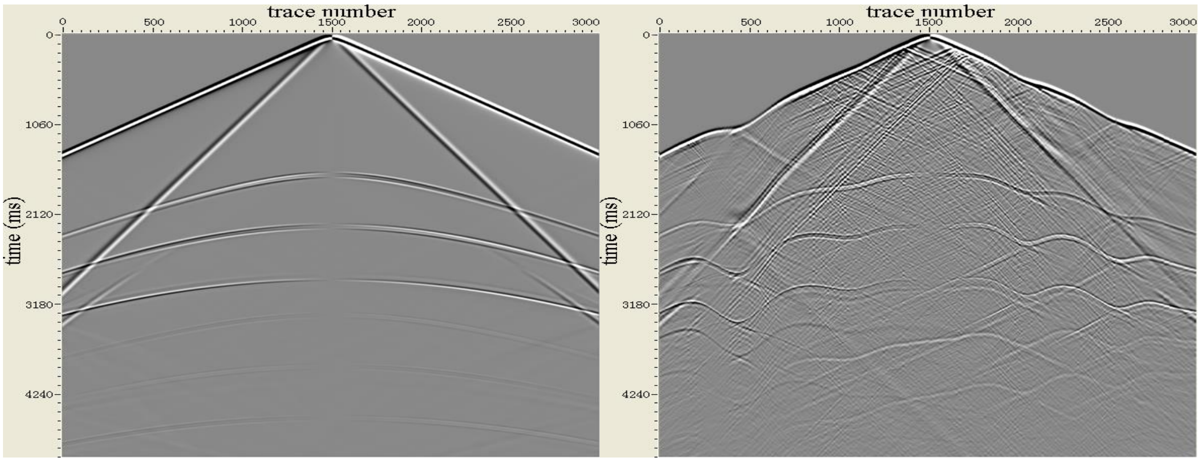

Figure 4 *Seismogram record of the velocity x components along the free surface in (a) the first simulation and (b) the second simulation.*

Conclusions

A 2D3C time-domain finite difference approximation was developed to model wave propagation in elastic and anisotropic media with an irregular free surface. We extend the image method from the existing elastic/viscoelastic isotropic media model to anisotropic media model. Numerical results show that modeling the subsurface as anisotropy media and removing the standard assumption of isotropy should lead to better understanding of wave fields that propagate in the Earth and to better methods of imaging the subsurface.

Acknowledgements

The work for this paper was supported by the Beijing Postdoctoral Scientific Research Funding Under Projects No. 2013ZZ-56.

References

Hestholm, S. O., and Ruud, B. O., 1994, 2d finite difference elastic wave modeling including surface topography: Geophys. Prosp., 42, 371-390.
Jih, R. S., McLaughlin, K. L., and Der, Z. A., 1988, Free-boundary conditions of arbitrary polygonal topography in a two-dimensional explicit elastic finite-difference scheme: Geophysics, 53, 1045-1055.
Levander, A. R., 1988, Fourth-order finite-difference P-SV seismograms: Geophysics, 53, 1425-1436.
Mittet, R., 2002, Free-surface boundary conditions for elastic staggered-grid modeling schemes: Geophysics, 67, 1616-1623.
Ohminato, T., and Chouet, B. A., 1997, A free-surface boundary condition for including 3D topography in the finite difference method: Bull. Seism. Soc. Am, 87, 494-515.
Robertsson, J. O. A., 1996, A numerical free-surface condition for elastic/viscoelastic finite-difference modeling in the presence of topography: Geophysics, 61, 1921-1934.
Wang, X. M., and Zhang H. L., 2004, Modeling of elastic wave propagation on a curved free surface using an improved finite-difference algorithm: Science in China, Ser.G., 47, 633-648.